First 40Ar/39Ar dating of intense Late Palaeogene lateritic weathering in Peninsular India

Nicolas J. Bonnet, Anicet Beauvais, Nicolas Arnaud, Dominique Chardon, Mudlappa Jayananda

▶ **To cite this version:**

Nicolas J. Bonnet, Anicet Beauvais, Nicolas Arnaud, Dominique Chardon, Mudlappa Jayananda. First 40Ar/39Ar dating of intense Late Palaeogene lateritic weathering in Peninsular India. Earth and Planetary Science Letters, 2014, 386, pp.126-137. 10.1016/j.epsl.2013.11.002 . hal-01097320

HAL Id: hal-01097320
https://hal.science/hal-01097320

Submitted on 2 Jan 2017

HAL is a multi-disciplinary open access archive for the deposit and dissemination of scientific research documents, whether they are published or not. The documents may come from teaching and research institutions in France or abroad, or from public or private research centers.

L'archive ouverte pluridisciplinaire **HAL**, est destinée au dépôt et à la diffusion de documents scientifiques de niveau recherche, publiés ou non, émanant des établissements d'enseignement et de recherche français ou étrangers, des laboratoires publics ou privés.

Revised manuscript
Click here to view linked References

First $^{40}Ar/^{39}Ar$ dating of intense Late Palaeogene lateritic weathering in Peninsular India

Nicolas Bonnet [1*], Anicet Beauvais [1], Nicolas Arnaud [2], Dominique Chardon [3,4,5], Mudlappa Jayananda [6]

[1] Aix-Marseille Université (AMU), IRD, CNRS, CEREGE UM34, BP 80, 13545 Aix-en-Provence, Cedex 4, France

[2] Université de Montpellier 2, Géosciences Montpellier, UMR CNRS 5243, 34095 Montpellier, France

[3] Université de Toulouse, UPS (OMP), GET,
14, avenue Edouard Belin, 31400 Toulouse, France

[4] CNRS, GET, 31400 Toulouse, France

[5] IRD, GET, 31400 Toulouse, France

[6] Department of Geology, Centre of Advanced Studies, University of Delhi, Delhi 110007, India

[*] Corresponding author: bonnet@cerege.fr

Abstract

Lateritic surface processes have shaped large platform and cratons of the tropical belt. Constraining the timing of such processes is crucial to decipher their role in cratonic morphogenesis and their response to long-term climatic change and lithospheric deformation. Weathering histories have been documented for South America, Africa and Australia, but precise time constraints of the lateritic weathering processes in South India are still lacking. We present $^{40}Ar/^{39}Ar$ ages of supergene cryptomelane (K-Mn oxide) formed in the Sandur Mn ore deposits exposed on the highest lateritic paleolandsurface that once covered the Mysore plateau and the adjacent Deccan Traps. Significant $^{40}Ar/^{39}Ar$ ages are estimated between ~ 36 and ~ 26 Ma from well-defined plateaus in step heating ^{39}Ar release spectra and from best-fitted inverse isochrones. These ages constitute firm time constraints that document intense late Eocene-Oligocene lateritic weathering over Peninsular India under the influence of warm and wet climate comparable to that prevailing in tropical humid forests. These results imply that Southern India was weathered between ~ 36 and 26 Ma and may have been dissected mostly in the Neogene.

Keywords: $^{40}Ar/^{39}Ar$ radiometric dating; Cryptomelane; Supergene Mn-ore deposits; Lateritic paleolandsurface; Sandur Greenstone Belt; South India

1. Introduction

Exposed laterites and lateritic duricrusts on relics of paleolandsurfaces in cratonic domains result from successive long-duration chemical weathering and erosion processes, and as such represent morphoclimatic fingerprints of tropical regions (Ollier, 1988; Bárdossy and Aleva, 1990; Thomas, 1994; Tardy and Roquin, 1998; Beauvais and Chardon, 2013). Since the first definition and description of laterites in South India (Buchanan, 1807), many studies were conducted on Indian lateritic formations (Subramanian and Mani, 1978; Babu, 1981; Sahasrabudhe and Deshmukh, 1981; Krishna Rao et al., 1989b; Widdowson and Cox, 1996; Widdowson and Gunnell, 1999), including manganiferous supergene ore deposits (Sawkar, 1981; Krishna Rao et al., 1982, 1989a; Dessai, 1985; Roy, 1992; Mohapatra et al., 1996; Sethumadhav et al., 2010). Except few geological stratigraphic constraints, radiometric dating of surface processes involved in the formation and evolution of Indian lateritic paleolandsurfaces are still lacking. Laterites are interlayered with marine sequences of late Eocene and early Miocene age (McGowran et al., 1977; Prasad, 1983). Lateritisation processes have also been indirectly dated with Neogene palynofossils found in colluvial/alluvial sediments overlying in-situ formed Mn ore deposits ~ 100 km south of Belgaum (Fig. 1). These fossils constrain intense weathering that led to Mn ore concentration to be Neogene at the latest (Krishna Rao et al., 1989a). The age of lateritic weathering has also been roughly estimated on the basis of the paleomagnetic properties of iron oxides formed in laterites around 16°N (Schmidt et al., 1983), i.e., “Early Tertiary” (Paleogene?) for the high-level Belgaum laterites and “Late Tertiary” (Neogene?) for the low-level laterites found west of the Western Ghats escarpment (Fig.1).

Chemical rock weathering commonly resulted in the accumulation of metallic elements (Al, Fe, Mn) in residual laterites and depletion of more soluble elements (Na, K, Si, Ca). Potassium, Na and/or Ba may, however, be retained by supergene Mn oxides in large crystallographic lacuna existing between the MnO_6 octahedra chains that define the typical tunnel-structure of the hollandite manganese oxide group. Cryptomelane belongs to this group with the general stoichiometric formulae $K_x Mn^{IV}_{8-x} Mn^{III}_x O_{16}$, x ranging from 0.2 to 1 and K_x counterbalancing Mn^{III} substitution for Mn^{IV} (Burns and Burns, 1979; Turner and Buseck, 1979; Post and Burnham, 1986; Pasero, 2005). Cryptomelane is a major Mn oxide of many lateritic Mn-ore deposits in South India (Sivaprakash and Phil, 1980; Krishna Rao et al., 1982; Mohapatra et al., 1996; Sethumadhav et al., 2010). This mineral hosts radioactive ^{40}K atoms, which can decay into ^{40}Ar. The high radiogenic ^{40}Ar retentive power of cryptomelane makes this mineral a suitable chronometer for $^{40}Ar/^{39}Ar$ step heating dating of weathering processes in lateritic soils including duricrusts and manganiferous ore deposits (Vasconcelos et al., 1992; Vasconcelos et al., 1994a; Ruffet et al., 1996; Vasconcelos, 1999).

This study quantifies the radiometric ages of lateritic weathering processes that have affected the rocks of the Dharwar craton on the Mysore Plateau by $^{40}Ar/^{39}Ar$ dating of cryptomelane from supergene Mn-ore deposits. We focus on the Fe-Mn sedimentary formations belonging to the Sandur Greenstone Belt (SGB) (Figs. 1 and 2a), which hosts the biggest Indian manganese reserve (Kameshwar et al., 2000). Our results provide tangible time constraints (Late Eocene – Oligocene) on the paleoweathering processes and morphoclimatic evolution of the potentially oldest lateritic paleolandsurface preserved on the Mysore plateau and Traps in southern India.

2. Geological and geomorphological setting

2.1. Sandur Greenstone Belt geology

The SGB is a synform-shape greenstone belt that consists of mafic/ultramafic volcanics and sediments (Fig. 2a) having undergone low-grade regional metamorphism during latest Archean orogeny that shaped the Dharwar craton (Roy and Biswas, 1979; Mukhopadhyay and Matin, 1993; Chadwick et al., 1996; Chardon et al., 2008). The sedimentary sequences contain elements of metavolcanic rock, which are relatively rich in Ni, Cr, Co and Sc. The upper part of the greenstone stratigraphic pile includes platform-like sediments bearing stromatolites, Mn formations and carbonaceous Mn phyllites (Fig. 2a).

In the eastern part of the belt, the upper part of the sequence includes banded iron formations (BIF), felsic volcanics and terrigenous sediments (Fig. 2a). SHRIMP U-Pb dating of zircon in two interlayered felsic volcanics indicate ages ranging from 2651 ± 18 Ma to 2659 ± 40 (Nutman et al., 1996). The BIF and Fe-Mn formations are related to marine transgression and regression cycles, respectively (Roy, 2006). These cycles implied alternating chemical and clastic sedimentation, which is also evidenced by specific iron formation facies and argillites within the BIF (Manikyamba et al., 1993). The lower part of the sequence is confined to the Deogiri region and is essentially composed of manganiferous stromatolitic limestones, dolomites and argillites (Fig. 2a) while the upper part is richer in Fe (Roy, 2000). Iron and Mn fractionation was controlled during eustatic sea-level variations by differentiated redox conditions of two stratified water masses on the shallow and deep shelf (Roy, 1992; Manikyamba and Naqvi, 1997). The Fe-Mn sediments have later been affected by low-grade metamorphism by 2475 ± 65 Ma (whole rock Pb/Pb isochron dating), which is the

maximal recrystallisation age of the limestones (Russell et al., 1996; Chadwick et al., 2000). Such a metamorphism led to Mn enrichment of the sediments (Roy, 2000), which are composed of Mn-carbonates, argillites, arenites and phyllites (Fig. 2a), and are the main protores of the SGB Mn-ore deposits. These deposits grade upward into supergene weathering materials (Roy, 2006).

2.2. Geomorphology of southern India and Sandur Greenstone Belt

The geomorphology of southern India consists of high-elevation surfaces occurring as relics of a differentiated landscape developed on the Dharwar craton and Deccan traps (Fig. 1), and low-elevation surfaces along the western coast (Radhakrishna, 1993), both being overlain by laterites (Widdowson and Cox, 1996; Widdowson, 1997). The regional eastern dip of the high-elevation surfaces is interpreted to result from eastward tilting of Peninsular India due to the Seychelles rifting and Deccan Traps events (~ 65-63 Ma) (Radhakrishna, 1993). On the Deccan Traps, bauxitic lateritic weathering of the highest preserved landsurface must be younger than 62.3 ± 0.6 Ma, which is the age of the youngest basalts (Courtillot et al., 1986; Pande, 2002). On the Traps and the Mysore Plateau, relics of two younger surfaces step below the plateau remnants of the high bauxitic surface (900-1000 m). The three erosion surfaces remain as sparse geomorphic relics at the scale of the Mysore plateau, and have been numbered S2, S3 and $S3_d$, the latter being a denudation degradation landform of S3 (Gunnell, 1998). Spatially reduced relics of the highest massifs also overhang the Mysore plateau (Fig. 1).

Landsurfaces S2, S3 and $S3_d$ are also identified on the SGB relief (Figs. 2b-c). The S2 surface levels the summits of the belt over an altitude range of 900 to 1100 m

and exposes deep in situ formed weathering mantles capped by Fe-Mn and Mn duricrusts at altitudes of ~ 1000-1016 m. Our study is mainly focused on the Mn ore open-pit mines carved in this surface (Figs. 2b-c). Relicts of paleo-land surface S3 extends below S2 over an altitude range of 750 to 850 m (Fig. 2c), and are covered by in-situ formed lateritic weathering profiles capped by iron duricrust instead of Mn ore concentrations. Relicts of land surface $S3_d$ occur as benches below the S3 surface over an altitude range of 700-750 m above the modern river network (Figs. 2c). The $S3_d$ surface is covered by reworked erosional materials including ferricrete and bedrock clasts originated from S3 lateritic profiles, sharing most characteristics with West African glacis/pediments (Beauvais and Chardon, 2013), but this surface is not affected by a late ferruginous or manganiferous lateritic duricrusting.

3. Material and methods

3.1. Ore bodies description and sampling

We have sampled across the main Mn ore bodies of the SGB deposits, which formed within weathered meta-sedimentary phyllites at different depths below the top of landsurface S2 at 1012-1015 m altitudes (Fig. 3). Description of samples precisely located on open-pit mine benches allowed the establishment of log sections (Fig. 3b and 3d). In Kappataswamy pit (N 14°59’59” E 76°32’42”, Fig. 3a), the first ore body was sampled between 856 and 893 m of elevation along the E-W log section 1 on the western benches of the pit, and the second one between 904 to 935 m along the N-S log section 2 on the eastern benches (Fig. 3b). The third ore body is located in Channanghi KMK-E pit (N 14°59’50’’ E 76°34’37’’, Fig. 3c) at an elevation range of 926 to 994 m (log section 3, Figure 3d). The Mn-ore bodies are composed of different petrographic

facies. The float and platty Mn-ores constitute the stratiform ore type, which is conformably bedded within weathered mangan-phyllites preserving this meta-sedimentary protore structure (Mishra, 1978). The massive Mn ore is found between ~ 850 m and 892 m elevation in the first section, between 904 m and 912 m elevation in the second ore body of the Kappataswamy pit (Fig. 3b), and between 926 and 982 m elevation in Channanghi KMK-E pit (Fig. 3d). The massive ore is a podiform type with cavity fillings (geodes) and botryoidal structures, which formed by secondary Mn supergene enrichments (Mishra, 1978). Iron-Mn duricrust of ~ 10 m thickness caps the two Mn-ore deposits immediately above a segregated/tabular ore body (Figs. 3b-d).

The samples collected in the Mn-ore deposits (Fig. 3b-d) were cut with a circular saw to get the best angle for mineralogical observations on metallographic quality polished thin sections (200-300 μm-thick) made from the sawed fragments (Fig. 4a). Symmetrically to the thin sections, 500 μm-thick slabs are prepared for sub-sampling of the target cryptomelane grains suitable for $^{40}Ar/^{39}Ar$ dating (Hénocque et al., 1998).

3.2. Analytical techniques and cryptomelane characterisation

Reflected light microscopy and X-ray micro fluorescence (μ-XRF) analyses allow precise characterisation of K-enriched Mn-oxide (cryptomelane) on the polished thin sections (Fig. 4b-c). Microscopic observations of thin sections were accomplished using a Leica DM-RXP microscope. The μ-XRF measurements were completed on slabs using a X-ray microscope (XGT7000, Horiba Jobin Yvon) equipped with a X-ray guide tube producing a finely focused and high-intensity beam with a 100 μm spot size, Rh X-ray tube, accelerating voltage of 30 kV and current of 1 mA. X-ray emission from the irradiated sample was detected via an energy dispersive X-ray (EDX) spectrometer

equipped with a liquid-nitrogen-cooled high purity Si detector. Micro mapping of the coupled Mn-K occurrences on slabs contributes to precise identification of cryptomelane, while Fe maps document the occurrence of Fe oxihydroxides (Fig. 4c). A Scanning electron microscope (SEM) has been also used for fine-scale observations of the cryptomelane crystals (Fig. 4d). Electron probe micro chemical analysis (EPMA) of minerals on polished thin sections was completed using a CAMECA SX-100 electron microprobe equipped with five wavelength-dispersive X-ray spectrometers (WDS).

Cryptomelane grains were separated from the slabs by hand picking. Cryptomelane separates were crushed to produce powders (< 64 μm), which were analyzed by XRD using a Panalytical X'Pert Pro MPD with a Co Kα X-ray source (λ = 1.79 Å) operating at 40 kV and 40 mA. The system is equipped with a linear X'Celerator detector and a flat monochromator. The analysis range was 10-85° 2θ with a step size of 0.033° and a counting time of 10 s per step.

After ultrasonically cleaning in absolute ethanol and conditioning in aluminium foil packets, other separated grains were irradiated for 50 hours in the TRIGA Mark-II reactor of Pavia University (Italia). The standard Taylor Creek Rhyolite sanidine 2 (TCRs-2) monitor, with an age of 28.05 Ma ± 0.08 (Baksi et al., 1996), was analysed after every ten unknown samples to allow determination of the factor J. After a two-month "cooling" period, the irradiated cryptomelane grains were loaded in a double vacuum Staudacher-type furnace for step heating Ar isotopes measurements. The furnace temperature was calibrated by means of a classical thermocouple, and the gas purification was accomplished using a cold trap with liquid air and Al–Zr AP10 getters (one hot, one cold) for 8 minutes before the introduction into the VG3600 mass spectrometer. One minute was allowed for equilibration before analysis. ^{40}Ar and ^{39}Ar

were measured on a Faraday cup with a resistor of 10^{11} ohm, while ^{39}Ar, ^{38}Ar, ^{37}Ar, and ^{36}Ar were analysed using a scintillator and photomultiplier after interaction on a Daly plate. The analytical data are reported in data repositories (Tables DR1 and DR2), and the errors are quoted at the 1σ level. Ages were analysed in two ways: plateaus and inverse isochrones. Plateaus ages were calculated from at least three consecutive steps comprising up to 50% of total $^{39}Ar_K$ released and overlapping at the 2σ confidence level (Fleck et al., 1977; Maluski, 1985). Alternatively, plateau ages encompassing two steps releasing ~ 30-40 % ^{39}Ar were also defined as "plateau-like" or "pseudo-plateau" (e.g., Feng and Vasconcelos, 2007; Vasconcelos et al., 2013). Ages derived from best-fit inverse isochrones in $^{36}Ar/^{40}Ar$ vs. $^{39}Ar/^{40}Ar$ correlation diagrams (Roddick et al., 1980) were accepted when mean square weighted deviation (MSWD) was less than 2.5 and the $^{40}Ar/^{36}Ar$ intercept within 2σ from the $(^{40}Ar/^{36}Ar)_{atm}$ value of 298.56 ± 0.31 (Lee et al., 2006; Renne et al., 2009), since supergene cryptomelane crystallised at shallow depth, and thus incorporated excess argon, if any, in the atmospheric ratio. Age spectra also show the variations of $^{40}Ar^*$ and K/Ca (derived from $^{39}Ar/^{37}Ar$) to track the compositional effects on age.

4. Results and Discussion

Six samples (KPA-2.1, KPA-2.5, KPA-9, KPA-10, KPA-12a and KPA-12b) from the Kappataswamy pit (Fig. 3b) and one (KMK-3) from the Channanghi KMK-E pit (Fig. 3d) were analysed and dated. KPA-9 and KPA-12 show the platy preserved meta-sedimentary structure with Mn pods, while KPA-2, KPA-10 and KMK-3 are rather massive with cavity crystallisations (geode) and/or botryoidal pod concretions.

242 4.1. Mineralogical and geochemical characterisation of cryptomelane

243 Cryptomelane was identified on polished thin sections including μ-XRF and
244 SEM imaging (Fig. 4), and characterized by microchemical (EPMA) and XRD analyses
245 of separated grains (Figs. 5 and 6, Table 1). Samples KPA-9, KPA-12a and KPA-12b
246 are the richest in cryptomelane, which occurs as cryptocrystalline plasmic domains
247 formed within preserved inherited protore microstructures (Figs. 5a-c). Appropriately,
248 sample KPA-9 exhibits a relict of Si-Mn sedimentary protore with residual smoothed
249 small size quartz grains preserved in acicular cryptocrystalline cryptomelane (Fig. 4d).
250 The two different generations of cryptomelane (Fig. 5a) have the same stoichiometric
251 composition (Table 1). Separated grain of KPA-9 mainly contains cryptomelane, but
252 also pyrolusite (βMnO_2) and quartz (Fig. 6). Sample KPA-12a is composed of two
253 cryptomelane generations, the latest one filling the micro porosity developed across the
254 earliest generation and/or the other mineral components such as pyrolusite and Fe
255 oxihydroxides (Fig. 5b). The stoichiometric composition is very close to that of KPA-9
256 (Table. 1). Sample KPA-12b is very rich in cryptomelane (Fig. 5c) with higher K
257 content than KPA-12a (Table. 1). The two separated grains are dominantly composed of
258 cryptomelane but pyrolusite and goethite ($\gamma FeOOH$) are also present (Fig. 6).
259 Samples KPA-2, KPA-10 and KMK-3 are composed of successive cryptomelane
260 crystallisations organized in banded overgrowth microstructures associated with other
261 Mn oxides (Figs. 5d-f and 6). In the sample KPA-2, the first three bands are pure
262 cryptomelane, the fourth is a cryptocrystalline mixture of nsutite and cryptomelane, and
263 the fifth is dominantly cryptomelane, while pyrolusite crystallized in a cavity (Fig. 5).
264 The cryptomelane crystals analysed in the different bands have different stoichiometric
265 compositions with K varying from 0.45 to 0.57 atoms (Table 1). Sample KPA-10

consists of a ~ 5 mm size cryptomelane concretion with a transition zone of less than 1 mm separating it from pyrolusite (Fig. 5e). Separated grain of KPA-10 is mainly composed of cryptomelane with 0.5 K atoms (Table 1). Small quantities of pyrolusite, goethite and hematite (Fe_2O_3) are also present (Fig. 6). Sample KMK-3 (Fig. 5f) is a concretion of cryptomelane with less than 1.5 wt.% K (Table 1). The outer rims are composed of lithiophorite $(Al,Li)MnO_2(OH)_2$ and nsutite (γMnO_2) (Fig. 5f), which also occur as minor fractions in the XRD analysis of the separated grain (Fig. 6).

4.2. $^{40}Ar/^{39}Ar$ ages of cryptomelane

Two kinds of $^{40}Ar/^{39}Ar$ age spectra are distinguished from the step heating degassing depending on their shape and interpretation. The first group displays regular ^{39}Ar release spectra allowing calculation of plateau ages (Fig. 7a-e), which are commonly defined at the 2σ error and accounting at least for 40% of the total ^{39}Ar released from the sample (Vasconcelos and Conroy, 2003; Feng and Vasconcelos, 2007; Beauvais et al., 2008). The second group corresponds to disturbed ^{39}Ar release spectra (Fig. 8), which are more problematic to interpret. The analytical data are provided in the data repository tables DR1 and DR2.

4.2.1. Regular $^{40}Ar/^{39}Ar$ age spectra

The $^{40}Ar/^{39}Ar$ age spectra from the first group have been obtained from the first generation of cryptomelane crystallized in the meta-sedimentary protore (Figs. 5a and 5c, 7a and 7c), and for cryptomelane crystallisations in banded overgrowth microstructures of botryoids (Figs. 5f and 7d) or geodes (Figs. 5d-e, 7b and 7e). In each

289 case the calculated plateau and pseudo-plateau ages agree with statistically meaningful
290 inverse isochron ages estimated in the correlation diagrams (Fig. 7).
291 However, these spectra present some anomalies at low and high temperatures
292 steps. The age spectrum of KPA-9 (Fig. 7a) shows younger individual ages (steps 10 to
293 13), which may reflect the degassing of a late cryptomelane crystallisation (Figs. 4b and
294 5a). The sample KPA-10 displays an age spectrum with a clear ascending "stair case"
295 pattern at low temperature (steps 1 to 7) with young ages affected by quite a large
296 standard deviation (Fig. 7b). The isochron suggests a moderate excess of ^{40}Ar, which
297 was interpreted as the result of primary mineral weathering (McDougall and Harrison,
298 1988; Vasconcelos et al., 1994a), which is unlikely in this sample (Figs. 5e and 7b,
299 Table 1). The higher amounts of released $^{40}Ar^{*}$ and ^{39}Ar in intermediate temperatures
300 (step 8 to 11), however, allow the best estimation of the cryptomelane crystallisation
301 age (Vasconcelos, 1999; Hautmann and Lippolt, 2000; Li and Vasconcelos, 2002;
302 Vasconcelos and Conroy, 2003; Feng and Vasconcelos, 2007). Sample KPA-12b is
303 characterised by well-constrained plateau and isochron ages (Fig.7c).
304 The age spectrum of KMK-3 exhibits an ascending "stair case" pattern at high
305 temperature (steps 8, 9, 10, 13 and 14) with older ages than the plateau age (Fig. 7d). In
306 such a case, it is usually admitted that radiogenic argon is released by two cryptomelane
307 phases, the older one retaining radiogenic ^{40}Ar better than the younger one (Feng and
308 Vasconcelos, 2007) resulting in a maximum plateau age estimate and an older
309 integrated age (Li and Vasconcelos, 2002). The plateau age of KMK-3 has also quite a
310 large error due to relatively low K content (Table 1 and Fig. 7d), and higher
311 atmospheric correction, the isochron being less sensible and thus more precise.

312 The age spectrum of KPA-2.1 (Fig. 7e) is more disturbed and does not allow
313 calculation of a standard plateau age (Fleck et al., 1977). Pseudo-plateaus ages have
314 been, however, previously estimated from similar spectra by considering only two
315 concordant steps including ~ 40% of ^{39}Ar released (e.g., Feng and Vasconcelos, 2007;
316 Vasconcelos et al., 2013). Two pseudo-plateaus occur in intermediate temperature steps
317 4-5 and 7-8, allowing for a concordant age estimate of 35.86 ± 1.10 Ma by combining
318 the four steps at the 2σ level (Fig. 7e). We note that the best-fitted isochron supports a
319 similar age (Fig. 7e). The high temperature steps 13 to 16 suggest a hypogene
320 contaminant (Vasconcelos et al., 1994a; Ruffet et al., 1996; Li and Vasconcelos, 2002),
321 which could have aged the intermediate steps (e.g., the step 6). The low K content
322 extraction in high temperature steps could have also suffered from imprecise blank
323 corrections. Therefore, similarly to the sample KMK-3 (Fig. 7d), the best-fitted isochron
324 might reasonably provide a more precise age (Fig. 7e).
325
326 *4.2.2. Disturbed ^{40}Ar/^{39}Ar age spectra*
327 The ^{39}Ar release spectra from the second group are characterized by an upward
328 convex shape (Fig. 8) suggestive of a mixing of two or more supergene cryptomelane
329 phases (Vasconcelos et al., 1995; Ruffet et al., 1996; Hautmann and Lippolt, 2000),
330 which may result from the handpicking of single grains. Phase mixing is obvious in
331 sample KPA-12a showing late cryptomelane crystallisation precipitated into the
332 porosity (≤ 500 μm) generated by the dissolution of a first plasmic cryptomelane
333 generation (Fig. 5b). Such a process may result in remobilization of low energy sites
334 (Colin et al., 2005; Beauvais et al., 2008). Phase mixing often occurs during separation
335 of grains from multiple overgrowth bands (Vasconcelos and Conroy, 2003). The grain

of KPA-2.5 was tentatively separated from a thin band (~ 500 μm) between a late pyrolusite crystallisation in a geodic void and a band composed of a mixing of cryptomelane and nsutite (Fig. 5d). The growth rate of cryptomelane crystals in banded overgrowth structures (botryoids or geodes) is generally very low (Vasconcelos et al., 1992; Dammer et al., 1996; Hénocque et al., 1998) and may result in vey small size (≤ 1 μm) intimately intergrown cryptomelane phases in a same grain (Vaconcelos et al., 1994b; Vasconcelos, 1999).

The pronounced upward convex shape of ^{39}Ar release spectra precludes plateau age calculation, while correlation diagrams only allow estimation of minimum and maximum ages of the oldest and youngest mixing phases, respectively (Fig. 8a-b). Each step of the ^{39}Ar release spectra yields a mixing age of the intergrown cryptomelane generations (Vasconcelos, 1999; Vasconcelos and Conroy, 2003; Feng and Vasconcelos, 2007), implying that the ages in low and high temperature steps are overestimates of the youngest phase, while the ages in intermediate temperature steps are underestimates of the oldest phase (see also Ruffet et al., 1996; Beauvais et al., 2008). This interpretation is mainly based on previous experiments (Vasconcelos et al, 1995), which showed a maximal degassing of ^{40}Ar* and ^{39}Ar between 700°C and 900°C with a peak at 800°C. In such a range of temperatures, the two isotopic components are release from the mineral structures (Vasconcelos et al., 1994b). Therefore, only maximum and minimum ages might be estimated from upward convex spectra in the temperature range specific of supergene cryptomelane degassing (Fig. 8). For KPA-2.5 (Fig. 8a), a minimum age of ~ 46 Ma (step 7) and a maximum age of ~ 30 Ma (step 10) could be at best estimated for the crystallisation of the earliest and latest cryptomelane phases, respectively. For KPA-12a the maximum and minimum ages of ~ 29 Ma (step

10) and ~ 34 Ma (step 8) are estimated for the youngest and oldest phases, respectively, in agreement with the estimated isochron age limits, although the MSWD value of the second isochron is quite large (Fig. 8b).

4.2.3. Cryptomelane $^{40}Ar/^{39}Ar$ ages summary

Despite mineral phase mixing of some samples, five significant plateau and isochron ages are estimated between ~ 26 and 36 Ma. The older ages (~ 33.5 and 36 Ma) are obtained either for the first cryptomelane generation in samples showing the preserved meta-sedimentary protore structure (Figs. 5a-c, 7a-c) or the first crystallisation band of an overgrowth geodic microstructure (Fig. 5d and 7e). The younger ages (~ 26-28 Ma) characterize the late cryptomelane crystallisations of banded overgrowth microstructures (Figs. 5e-f, 7b and 7d). The ages of the different mixing phases of KPA-2.5 and KPA-12a cannot be precisely determined. However, the two cryptomelane phase of KPA-12a (Fig. 5b) may have crystallised between ~ 29 Ma and ~ 34 Ma (Fig. 8c) that bracket the age of KPA-12b (Fig. 7c) sampled on the same open mine bench. The maximum age (~ 30 Ma) estimated for the youngest cryptomelane of KPA-2.5 is quite realistic compared to the older cryptomelane grain (KPA-2.1) separated from the same sample (Fig. 5d and 7e). Despite their limited number, our results usefully document Late Paleogene weathering history of southern India.

4.3. Potential implications for lateritic weathering and morphogenesis in southern India

The formation of cryptomelane in Mn-ore deposits is enhanced on landsurfaces covered by a humid tropical forest reflecting warm and/or at least wet climatic conditions (Vasconcelos et al., 1994a), like those prevailing for bauxite genesis in

384 tropical cratonic regions (Bárdossy and Aleva, 1990). Such hydroclimatic conditions are
385 required for complete weathering of K-phyllosilicates into kaolinite with release of K^+
386 in Mn^{2+}-rich acidic solutions (pH ~ 4.5-5) that may ultimately lead to cryptomelane
387 crystallisation under appropriate redox conditions (Parc et al., 1989). Therefore, massive
388 formation of cryptomelane in Mn ore deposits and/or lateritic weathering profiles is a
389 good indicator of humid/warm paleoclimatic conditions (Vasconcelos et al., 1994a;
390 Vasconcelos and Conroy, 2003; Beauvais et al., 2008). Under such climatic conditions,
391 wide areas were colonised by humid tropical forests over most of peninsular India (Kent
392 and Muttoni, 2008; Chatterjee et al., 2013) enhancing the pervasive development of
393 lateritic weathering profiles with differential sequestration of Al, Fe and Mn.
394 On the basis of global paleoclimatic reconstructions (e.g., Parrish et al., 1982),
395 Bárdossy and Aleva (1990) argued for intermittent Cenozoic bauxitic weathering in
396 South India. Such a bauxitic weathering intermittency was not observed in West Africa,
397 where bauxites preserved in current landscapes have been dated from Late Palaeocene
398 to Eocene at the latest (Prasad, 1983; Colin et al., 2005; Beauvais et al., 2008; Beauvais
399 and Chardon, 2013). Nevertheless, two stages of lateritic weathering processes have
400 been described in the bauxitic deposits of the Boknur-Navge plateau near Belgaum
401 (Krishna Rao et al., 1989b) (Fig. 1). The first bauxitic stage characterizes the syngenetic
402 lateritic weathering of the Deccan basalts under the action of slightly acidic meteoric
403 waters, whereas the second stage is a late weathering epigenetic process of the early
404 bauxite, under the effect of highly acidic meteoric Si-rich waters (Krishna Rao et al.,
405 1989b). The Boknur-Navge bauxitic plateau is also a remnant of paleolandsurface S2
406 correlated to the S2 remnant of the SGB (Gunnell, 1998). Syngenetic bauxitic
407 weathering on paleolandsurface S2 was likely active in the “Early Tertiary” (Paleogene

?) as suggested by paleomagnetic investigations on Fe-oxihydroxides in bauxites and laterites of the nearby Belgaum area (Schmidt et al., 1983; Kumar, 1986). Although no precise ^{40}Ar-^{39}Ar age correlative of syngenetic bauxitic weathering of the Traps basalts was obtained in this study, lateritic weathering up to ~ 46 Ma may not be precluded (Fig. 8a). Epigenetic lateritic weathering of paleolandsurface S2 (Krishna Rao et al., 1989b) could however be recorded by our $^{40}Ar/^{39}Ar$ ages set.

The obtained ages (~26, ~ 28, ~ 33.5 and ~ 36 Ma) attest for intense Late Eocene to Mid-Oligocene lateritic weathering(s) of the highest paleolandsurface (S2) preserved as sparse relics on both the Mysore plateau and the Deccan Traps. These results suggest that the high-elevation landsurface of Peninsular India evolved under a wet and warm climate over a protracted period in the Late Paleogene, essentially during the Oligocene. Repeated lateritic weathering between 26 and 36 Ma apparently correlates with low clastic sediment fluxes and dominant carbonate sedimentation on the Arabian sea margin (Campanile et al., 2008) but the links between inland weathering, erosion and offshore sedimentation are poorly understood. Our $^{40}Ar/^{39}Ar$ results might also suggest that the dissection and rejuvenation of the high-elevation lateritic surface of Peninsular India took place in the Neogene as classically inferred (Radhakrishna, 1993). However, the relative contributions of lithospheric deformation and climate change to geomorphic rejuvenation of Peninsular India in the Neogene remain to be investigated.

5. Conclusion

We provide time constraints on lateritic weathering having affected Southern India by using $^{40}Ar/^{39}Ar$ radiometric dating of supergene cryptomelane in Mn ore deposits underlying a relict paleolandsurface (S2) that once covered the Mysore plateau

and Deccan Traps. Well-constrained plateau ages and best-fitted inverse isochrons allow defining $^{40}Ar/^{39}Ar$ ages at ~ 26, ~ 28, ~ 33.5 and ~ 36 Ma. These results document intense lateritic weathering in Southern India during the latest Eocene and the Oligocene under the effect of warm and wet climate similar to that prevailing in humid forest tropical environments. More specifically, the highest regional lateritic paleolandsurface (S2) of Peninsular India underwent chemical weathering at least between ~ 36 and ~ 26 Ma and was possibly dissected and rejuvenated afterwards, which suggests that most of the current relief of South Indian high-elevation terrains was acquired in the Neogene.

Acknowledgements

We are thankful to the PhD school (ED251, AMU, OSU Pytheas), which allocated to NB a grant from the French Ministry of Research and Superior Education. We also thank IRD and INSU for financial supports (AB). Bujkesh was our guide during a three weeks field trip. S.R. Sridhar, M.P. Deshpande and K. Raman are gratefully thanked to having allowed us the sampling of the Deogiri Mn ore deposits. Thanks to the assistance of Prakash Babu in the mining open pits. C. Demeurie (Thin section Lab) made the polished thin sections. This work also benefited of technical helps from D. Borschneck (XRD and μXRF), Y. Galy (SEM), J-P. Ambrosi (chemical supplies), D. Merlet (EPMA), P. Münch and F. Lecoeur (Argon radiochronology). Jason Price and an anonymous reviewer are also thanked for useful remarks and suggestions.

456 **References**

457 Babu, P.V.L.P., 1981. Laterite as an unconformity plane in the evolution of the South
458 Indian peninsula – a synthesis, International Seminar on Lateritisation Processes
459 (Trivandrum, India 11-14 December, 1979). Balkema, A. A., Rotterdam, pp. 302-
460 307.

461 Baksi, A.K., Archibald, D.A., Farrar, E., 1996. Intercalibration of $^{40}Ar^{39}Ar$ dating
462 standards. Chem. Geol. 129, 307-324. doi: 10.1016/0009-2541(95)00154-9

463 Bárdossy, G., Aleva, G.J.J., 1990. Lateritic bauxites. Elsevier, Amsterdam, The
464 Netherlands.

465 Beauvais, A., Chardon, D., 2013. Modes, tempo, and spatial variability of Cenozoic
466 cratonic denudation: The West African example. Geochemis. Geophys. Geosyst.
467 14, 1590-1608. doi: 10-1002/ggge.20093

468 Beauvais, A., Ruffet, G., Hénocque, O., Colin, F., 2008. Chemical and physical erosion
469 rhythms of the West African Cenozoic morphogenesis: The ^{39}Ar-^{40}Ar dating of
470 supergene K-Mn oxides. J. Geophys. Res. - Earth Surf. 113, F04007. doi:
471 10.1029/2008jf000996

472 Buchanan, F., 1807. A journey through the countries of Mysore, Canara and Malabar.
473 Asian Educational Services, New-Delhi, India.

474 Burns, R.G., Burns, V.M., 1979. Manganese oxides, Marine Minerals. Mineral. Soc.
475 Am., 1-46.

476 Campanile, D.J., Nambiar, C.G., Bishop, P., Widdowson, M., Brownn, R., 2008.
477 Sedimentation record in the Konkan Kerala Basin: implications for the evolution
478 of theWestern Ghats and the Western Indian passive margin. Basin Res. 20, 3-22.
479 doi: 10.1111/j.1365-2117.2007.00341.x

480 Chadwick, B., Vasudev, V., Ahmed, N., 1996. The Sandur schist belt and its adjacent
481 plutonic rocks implications for Late Archaean crustal evolution in Karnataka. J.
482 Geol. Soc. India 47, 635-639.
483 Chadwick, B., Vasudev, V.N., Hegde, G.V., 2000. The Dharwar craton, southern India,
484 interpreted as the result of Late Archaean oblique convergence. Precamb. Res. 99,
485 91-111.
486 Chardon, D., Jayananda, M., Chetty, T.R., Peucat, J.-J., 2008. Precambrian continental
487 strain and shear zone patterns: South Indian case. J. Geophys. Res. 113, B08402.
488 doi: 10.1029/2007JB005299
489 Chatterjee, S., Goswami, A., Scotese, C.R., 2013. The longest voyage: Tectonic,
490 magmatic, and paleoclimatic evolution of the Indian plate during its northward
491 flight from Gondwana to Asia. Gondwana Res. 23, 238-267. doi:
492 10.1016/j.gr.2012.07.001
493 Colin, F., Beauvais, A., Ruffet, G., Hénocque, O., 2005. First $^{40}Ar/^{39}Ar$ geochronology
494 of lateritic manganiferous pisolites: Implications for the Palaeogene history of a
495 West African landscape. Earth Planet. Sci. Lett. 238, 172-188. doi:
496 10.1016/j.epsl.2005.06.052
497 Courtillot, V., Besse, J., Vandamme, D., Montigny, R., Jaeger, J.-J., Cappetta, H., 1986.
498 Deccan flood basalts at the Cretaceous/Tertiary boundary? Earth Planet. Sci. Lett.
499 80, 361-374.
500 Dammer, D., Chivas, A., McDougall, I., 1996. Isotopic dating of supergene manganese
501 oxides from the Groote Eylandt deposit, Northern territory, Australia. Econ. geol.
502 91, 386-401.

503 Dessai, A., 1985. An appraisal of the manganese ore deposits of Goa, India.
504 Proceedings of the Indian National Science Academy, Part A. Physical sciences
505 51, 1021-1032.
506 Feng, Y.X., Vasconcelos, P.M., 2007. Chronology of Pleistocene weathering processes,
507 southeast Queensland, Australia. Earth Planet. Sci. Lett. 263, 275–287.
508 doi:10.1016/j.epsl.2007.08.036
509 Fleck, R.J., Sutter, J.F., Elliot, D.H., 1977. Interpretation of discordant $^{40}Ar/^{39}Ar$ age-
510 spectra of mesozoic tholeiites from antarctica. Geochim. Cosmochim. Acta 41,
511 15-32.
512 Gunnell, Y., 1998. The interaction between geological structure and global tectonics in
513 multistoreyed landscape development: a denudation chronology of the South
514 Indian shield. Basin Res. 10, 281-310.
515 Hautmann, S., Lippolt, H.J., 2000. $^{40}Ar/^{39}Ar$ dating of central European K-Mn oxides a
516 chronological framework of supergene alteration processes during the Neogene.
517 Chem. Geol. 170(1-4), 37-80.
518 Hénocque, O., Ruffet, G., Colin, F., Féraud, G., 1998. $^{40}Ar/^{39}Ar$ dating of West African
519 lateritic cryptomelanes. Geochim. Cosmochim. Acta 62, 2739-2756.
520 Kameshwar, D.R., Thambi, P.I., Srinivasamurthy, V., Sheriff, M.A.N.A., Shanmugam,
521 P., Chayapathi, N., Panduranga, R., Jagannathachar, L.G., Naik, R.H.,
522 Vidyadharan, K.T., 2000. Final report on Sandur manganese exploration, Bellary
523 district, Karnataka. Unpub. Prog. Rep. Geol. Surv. Ind. For the FS 54, 411-414.
524 Kent, D.V., Muttoni, G., 2008. Equatorial convergence of India and early Cenozoic
525 climate trends. Proc. Nat. Acad. Sci. 105, 16065-16070. doi:
526 10.1073/pnas.0805382105

527 Krishna Rao, B., Muzamil Ahmed, M., Janardhana, M.R., 1989a. Age of manganiferous
528 laterite of Uttara Kanada district, Karnataka. J. Geol. Soc. India 34, 413-420.
529 Krishna Rao, B., Satish, P.N., Sethumadhav, M.S., 1989b. Syngenetic and Epigenetic
530 features and genesis of the beauxite-bearing laterite of Boknur-Navge, Belgaum
531 district, Karnataka. J. Geol. Soc. India 34, 46-60.
532 Krishna Rao, B., Srinivasan, R., Ramachandra, B.L., Sreenivas, B.L., 1982. Mode of
533 occurrence and origin of manganese ores of Shimoga district, Karnataka. J. Geol.
534 Soc. India 23, 226-235.
535 Kumar, A., 1986. Palaeolatitudes and the age of Indian laterites. Palaeogeogr.
536 Palaeoclim. Palaeoecol. 53, 231-237.
537 Lee J-Y, Marti, K., Severinghaus, J.P., Kawamura, K., Yoo, H-S., Lee, J.B., Kim, J.S.,
538 2006. A redetermination of the isotopic abundances of atmospheric Ar. Geochim.
539 Cosmochim. Acta 70, 4507–4512. doi:10.1016/j.gca.2006.06.1563
540 Li, J.W., Vasconcelos, P.M., 2002. Cenozoic continental weathering and its
541 implications for the palaeoclimate: evidence from $^{40}Ar/^{39}Ar$ geochronology of
542 supergene K–Mn oxides in Mt Tabor, central Queensland, Australia. Earth Planet.
543 Sci. Lett. 200, 223–239. doi:10.1016/j.epsl.2007.01.021
544 Maluski, H., 1985. Méthode Argon 39 - Argon 40 : Principe et applications aux
545 minéraux des roches terrestres. Masson, Paris, France.
546 Manikyamba, C., Balaram, V., Naqvi, S.M., 1993. Geochemical signatures of
547 polygenetic origin of a banded iron formation (BIF) of the Archean Sandur
548 greenstone belt (schist belt) Karnataka nucleus, India. Precamb. Res. 61, 137-164.

549 Manikyamba, C., Naqvi, S.M., 1997. Mineralogy and geochemistry of Archaean
550 greenstone belt-hosted Mn formations and deposits of the Dharwar Craton: Redox
551 potential of proto-oceans. Geol. Soci., London, Spec. Publi. 119, 91-103.
552 McDougall, I., Harrison, T.M., 1988. Geochronology and thermochronology by the
553 $^{40}Ar/^{39}Ar$ method. Oxford Univ. Press., New York.
554 McGowran, B., Rutland, R.W.R., Twidale, C.R., 1977. Discussion: Age and origin of
555 laterite and silcrete duricrusts and their relationship to episodic tectonism in the
556 mid-north of South Australia. J. Geol. Soc. Australia 24, 421-422.
557 Mishra, R.N., 1978. Exploration planing for Sandur manganese ores. J. Geol. Soc. India
558 19, 446-453.
559 Mohapatra, B.K., Rao, D.S., Nayak, B.D., Sahoo, R.K., 1996. Mineralogical and
560 chemical characteristics of ferromanganese ores from Sandur, Karnataka, India. J.
561 Miner. Petrol. Econ. Geol. 91, 46 - 61.
562 Mukhopadhyay, D., Matin, A., 1993. The structural anatomy of the Sandur schist belt—
563 a greenstone belt in the Dharwar craton of South India. J. Struc. Geol. 15, 309-
564 322.
565 Nutman, A.P., Chadwick, B., Krishna Rao, B., Vasudev, V.N., 1996. SHRIMP U/Pb
566 zircon ages of acid volcanic rocks in the Chitradurga and Sandur Groups and
567 granites adjacent to the Sandur Schist Belt, Karnataka. J. Geol. Soc. India 47, 153-
568 164.
569 Ollier, C.D., 1988. Deep Weathering, Groundwater and Climate. Geog. Annal. Series A,
570 Physic. Geog. 70, 285-290.
571 Pande, K., 2002. Age and duration of the Deccan Traps, India: A review of radiometric
572 and paleomagnetic constraints. J. Earth Syst. Sci. 111, 115-123.

573 Parc, S., Nahon, D., Tardy , Y., Vieillard, P., 1989. Estimated solubility products and
574 field of stability for cryptomelane, nsutite, birnessite and lithiophorite based on
575 natural lateritic weathering sequences. Am. Mineral. 74, 466-475.
576 Parrish, J.T., Ziegler, A., Scotese, C.R., 1982. Rainfall patterns and the distribution of
577 coals and evaporites in the Mesozoic and Cenozoic. Palaeogeogr. Palaeoclim.
578 Palaeoecol. 40, 67-101.
579 Pasero, M., 2005. A short outline of the tunnel oxides. Rev. Miner. Geochem. 57, 291-
580 305. doi:10.2138/rmg.2005.57.9
581 Post, J.E., Burnham, C.W., 1986. Modeling tunnel-cation displacements in hollandites
582 using structure-energy calculations. Am. Mineral. 71, 1178-1185.
583 Prasad, G., 1983. A review of the early Tertiary bauxite event in South America, Africa
584 and India. J. Afric. Earth Sci. (1983) 1, 305-313.
585 Radhakrishna, B.P., 1993. Neogene uplift and geomorphic rejuvenation of the Indian
586 Peninsula. Current Science 64(11/12), 787-793.
587 Renne, P.R., Cassata, W.S., Morgan, L.E., 2009. The isotopic composition of
588 atmospheric argon and 40Ar/39Ar geochronology: time for a change. Quat.
589 Geochron. 4, 288-298.
590 Roddick, J.C., Cliff, R.A., Rex, D.C., 1980. The evolution of excess argon in alpine
591 biotites A^{40}-Ar^{39}Ar analysis. Earth Planet. Sci. Lett. 48, 185-208.
592 Roy, S., 1992. Environments and processes of Manganese Deposition. Econ. Geol. 87,
593 1218-1236.
594 Roy, S., 2000. Late Archean initiation of manganese metallogenesis: its significance
595 and environmental controls. Ore Geol. Rev. 17, 179-198.

596 Roy, S., 2006. Sedimentary manganese metallogenesis in response to the evolution of
597 the Earth system. Earth-Sci. Rev. 77, 273-305. doi:
598 10.1016/j.earscirev.2006.03.004
599 Roy, S., Biswas, S.K., 1979. Metamorphic history of the Sandur schist belt, Karnataka.
600 J. Geol. Soc. India 20, 179-187.
601 Ruffet G., Innocent, C., Michard, A., Féraud, G., Beauvais, A., Nahon, D., Hamelin, B.,
602 1996. A geochronological $^{40}Ar/^{39}Ar$ and $^{87}Rb/^{87}Sr$ study of K-Mn oxides from the
603 weathering sequence of Azul (Brazil). Geochim. Cosmochim. Acta 60, 2219-
604 2232.
605 Russell, J., Chadwick, B., Rao, B.K., Vasudev, V.N., 1996. Whole-rock Pb/Pb isotopic
606 ages of Late Archaean limestones, Karnataka, India. Precamb. Res. 78, 261-272.
607 Sahasrabudhe, Y.S., Deshmukh, S.S., 1981. The laterites of the Maharashtra State.
608 Lateritisation processes, International Seminar on Lateritisation Processes
609 (Trivandrum, India 11-14 December, 1979). Balkema, A. A., Rotterdam, pp. 209-
610 220.
611 Sawkar, R.H., 1981. Geology of the manganese ore deposits of North Kanara district,
612 Karnataka state, India, in: Varentsov, I.M. (Ed.), Manganese Deposits on
613 Continents, 2 ed. Grassely, London, pp. 279-295.
614 Schmidt, P.W., Prasad, V., Ramam, P.K., 1983. Magnetic ages of some Indian laterites.
615 Palaeogeogr. Palaeoclim. Palaeoecol. 44, 185-202.
616 Sethumadhav, M.S., Gunnell, Y., Ahmed, M.M., Chinnaiah, 2010. Late Archean
617 manganese mineralization and younger supergene manganese ores in the Anmod–
618 Bisgod region, Western Dharwar Craton, southern India: Geological

619 characterisation, palaeoenvironmental history, and geomorphological setting. Ore
620 Geol. Rev. 38, 70-89. doi: 10.1016/j.oregeorev.2010.06.001
621 Sivaprakash, C.B., Phil, D., 1980. Mineralogy and geochemistry of some manganese-
622 iron deposits, Karnataka, India. Trans. Inst. Min. Metal., Section B-applied Earth
623 Science 90, 174-182.
624 Subramanian, K.S., Mani, G., 1978. Geomorphic significance of bauxite below Mio-
625 Pliocene sediments in the West Coast. Symp. Morph. Evol. Landforms, Dec.
626 1978, New Delhi, 83-87.
627 Tardy , Y., Roquin, C., 1998. Dérive des continents paleoclimats et altérations
628 tropicales. BRGM, Orléans, France.
629 Thomas, M.F., 1994. Geomorphology in the tropics. A study of weathering and
630 denudation in low latitudes. John Wiley & Sons Ltd, Chichester, England.
631 Turner, S., Buseck, P.R., 1979. Manganese Oxide Tunnel Structures and Their
632 Intergrowths. Science 203, 456-458.
633 Vasconcelos, P., 1999. K-Ar and $^{40}Ar/^{39}Ar$ geochronology of weathering processes.
634 Annu. Rev. Earth Planet. Sci. 27, 183-229.
635 Vasconcelos, P.M., Becker, T.A., Renne, P.R., Brimhall, G.H., 1992. Age and duration
636 of weathering by ^{40}K-^{40}Ar and ^{40}Ar-^{39}Ar analysis of supergene potassium-
637 manganese oxides. Science 258, 451-455.
638 Vasconcelos, P.M., Conroy, M., 2003. Geochronology of weathering and landscape
639 evolution, Dugald River valley, NW Queensland, Australia. Geochim.
640 Cosmochim. Acta 67(16), 2913–2930. doi:10.1016/S0016-7037(02)01372-8
641 Vasconcelos, P.M., Heim, J.A., Farley, K.A., Monteiro, H., Waltenberg, K., 2013.
642 $^{40}Ar/^{39}Ar$ and (U-Th)/He - $^{4}He/^{3}He$ geochronology of landscape evolution and

channel iron deposit genesis at Lynn Peak, Western Australia. Geochim. Cosmochim. Acta 117, 283-312. doi: 10.1016/j.gca.2013.03.037

Vasconcelos, P.M., Renne, P.R., Becker, T.A., Wenck, H.R., 1995. Mechanisms and kinetics of atmospheric, radiogenic, and nucleogenic argon release from cryptomelane during $^{40}Ar/^{39}Ar$ analysis. Geochim. Cosmochim. Acta 59, 2057-2070.

Vasconcelos, P.M., Renne, P.R., Brimhall, G.H., Becker, T.A., 1994a. Direct dating of weathering phenomena by $^{40}Ar^{39}Ar$ and K-Ar analysis of supergene K-Mn oxides. Geochim. Cosmochim. Acta 58, 1635-1665.

Vasconcelos, P.M., Wenck, H-R., Echer, C., 1994b. In situ study of the thermal behavior of cryptomelane by high-voltage and anlytical electron microscopy. Amer. Miner. 79(1-2), 80-90.

Widdowson, M., 1997. Tertiary paleosurfaces of the SW Deccan, Western India: implication for passive margin uplift, in: Widdowson, M. (Ed.), Palaeosurfaces: recognition, Reconstruction and Palaeoenvironmental Interpretation. Geological Society Special Publication, London, pp. 221-248.

Widdowson, M., Cox, 1996. Uplift and erosional history of the Deccan Traps, India: Evidence from laterites and drainage patterns of the Western Ghats and Konkan Coast. Earth Planet. Sci. Lett. 137, 57-69.

Widdowson, M., Gunnell, Y., 1999. Tertiary palaeosurfaces and lateritization of the coastal lowlands of western peninsula India, in: Thiry, M., Simon-Coinçon, R. (Eds.), Palaeoweathering, Palaeosurfaces and Related Continental Deposits. International Association of Sedimentologists, Special Publication, pp. 245-274.

Figures and table caption

Figure 1. Simplified map of Peninsular India showing first-order geomorphic and geological features (adapted from Radhakrishna, 1993). B= Bababudan; N= Nilghiris; S= Shevaroy.

Figure 2. Simplified geology of the Sandur Greenstone Belt adapted from Chadwick et al. (1996). (b) Corresponding topography (ASTER GDEM30) and delineation of relicts of paleosufaces S2 and S3. (c) Topographic cross-sections (lines of section are located on Figure 2b).

Figure 3. North-looking Google Earth views of (a) Kappataswamy and (b) Channanghi KMK-E pits showing the location of the cross-sections through the Mn ore bodies. (c) Logs of sections 1 and 2. (d) Log of section 3. Black numbered samples are those analysed and dated in the current study.

Figure 4. Characterisation of procedure used for separating cryptomelane grains in samples. (a) Polished thin section observed by (b) reflected light microscopy and (c) X-ray micro fluorescence, which yields a composite picture with Mn in blue, K in green and Fe in red. (d) SEM image showing typical cryptomelane acicular crystals in a composite weathering matrix, which preserves altered quartz grains of the protore. P = pyrolusite; C = cryptomelane; Pr = protore; Q = quartz.

Figure 5. Reflected-light photomicrographs of mineral assemblages of dated samples showing EPMA numbered targets. (a) Two generations of cryptomelane (C1, C2) and Pyrolusite (P) formed into the Mn protore (Pr). (b) Coexistence of two generations of cryptomelane (C1, C2) with pyrolusite (P) and Fe-oxihydroxide (Fe). (c) Crypomelane

(C) and pyrolusite with some Fe-oxihydroxides (Fe). (d) Cavity filling by banded overgrowth of a succession of cryptomelane (C) with pyrolusite (P) and a mixed overgrowth on nsutite+ cryptomelane (NC). (e) Massive cryptomelane and pyrolusite with some oxihydroxides (Fe). (f) Massive banded overgrowth of cryptomelane (C) with pyrolusite (P), lithiophorite (L) and nsutite. Sample names are reported on each photomicrograph.

Figure 6. X-ray diagrams of separated cryptomelane sub-samples. C = cryptomelane; L = lithiophorite; n = nsutite; Q = quartz; p = pyrolusite; G = goethite; h = hematite

Figure 7. ^{39}Ar-^{40}Ar age spectra showing a well-defined plateau, with K/Ca (black) and Ar* (grey) step curves (left), and inverse isochrone diagrams (right) of cryptomelane separates from Kappataswamy open pit samples (a-c and e), and Channanghi KMK-E open pit sample (d). MSWD = mean square weighted deviation.

Figure 8. Disturbed ^{39}Ar-^{40}Ar age spectra with K/Ca (black) and Ar* (grey) step curves (left) and inverse isochrone diagrams (right) of cryptomelane separates from Kappataswamy open pit samples. (a) Separated phase of KPA-2.5 (target 5 in Figure 5d). Samples KPA-2.5 and KPA-12a do not allow calculation of plateau age but only maximum and minimum ages of the mixed youngest and oldest phases, respectively (stippled line depicted from bold numbered steps in the spectra). MSWD = mean square weighted deviation.

Table 1. Electron Probe Micro Analyses (EPMA) of targeted cryptomelane phases (in bold) and other Mn oxides shown in the Figure 5. Each analyse is the average of three 5μm micro spots in a 50 μm sized micro domain.

Highlights

* First radiochronological dating of lateritic weathering in southern India

* Late Palaeogene chemical weathering on the highest paleolandsurface preserved on the Mysore plateau and Deccan Traps

* Potential rejuvenation and acquisition of the current relief of southern India in the Neogene

Figure. 1

Click here to download Figure: Figure. 1(EPSL-D-13-00742).pdf

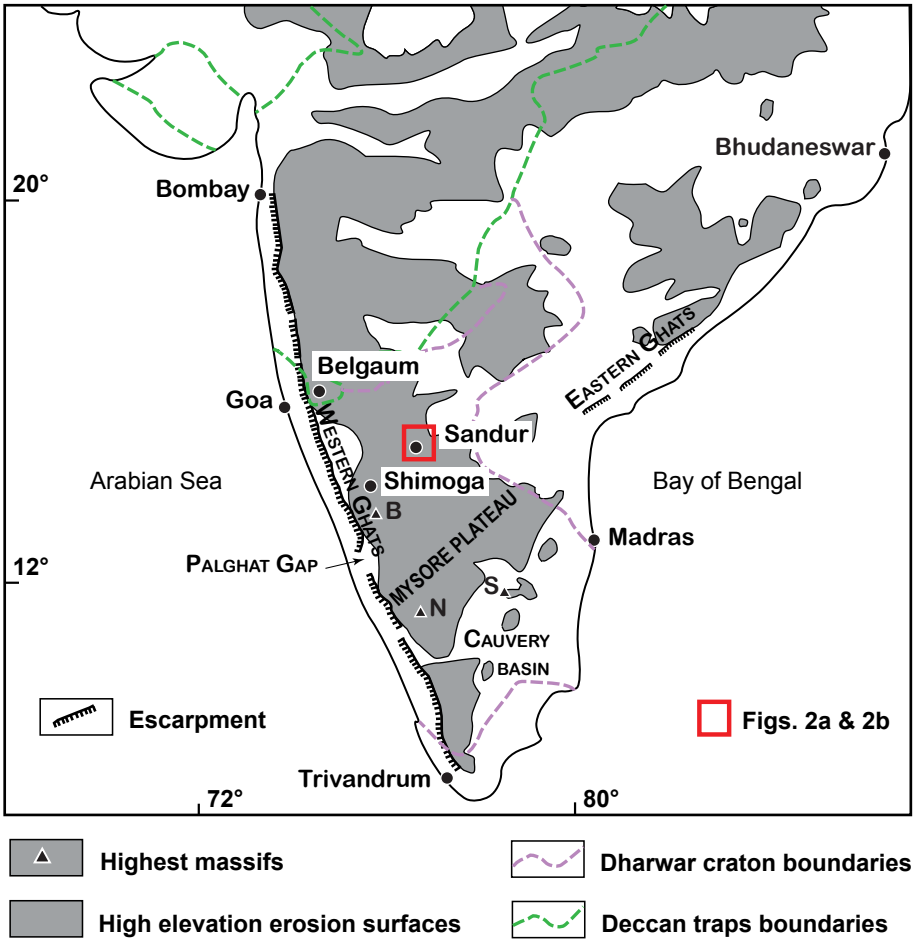

FIG. 1

Figure. 2

Click here to download high resolution image

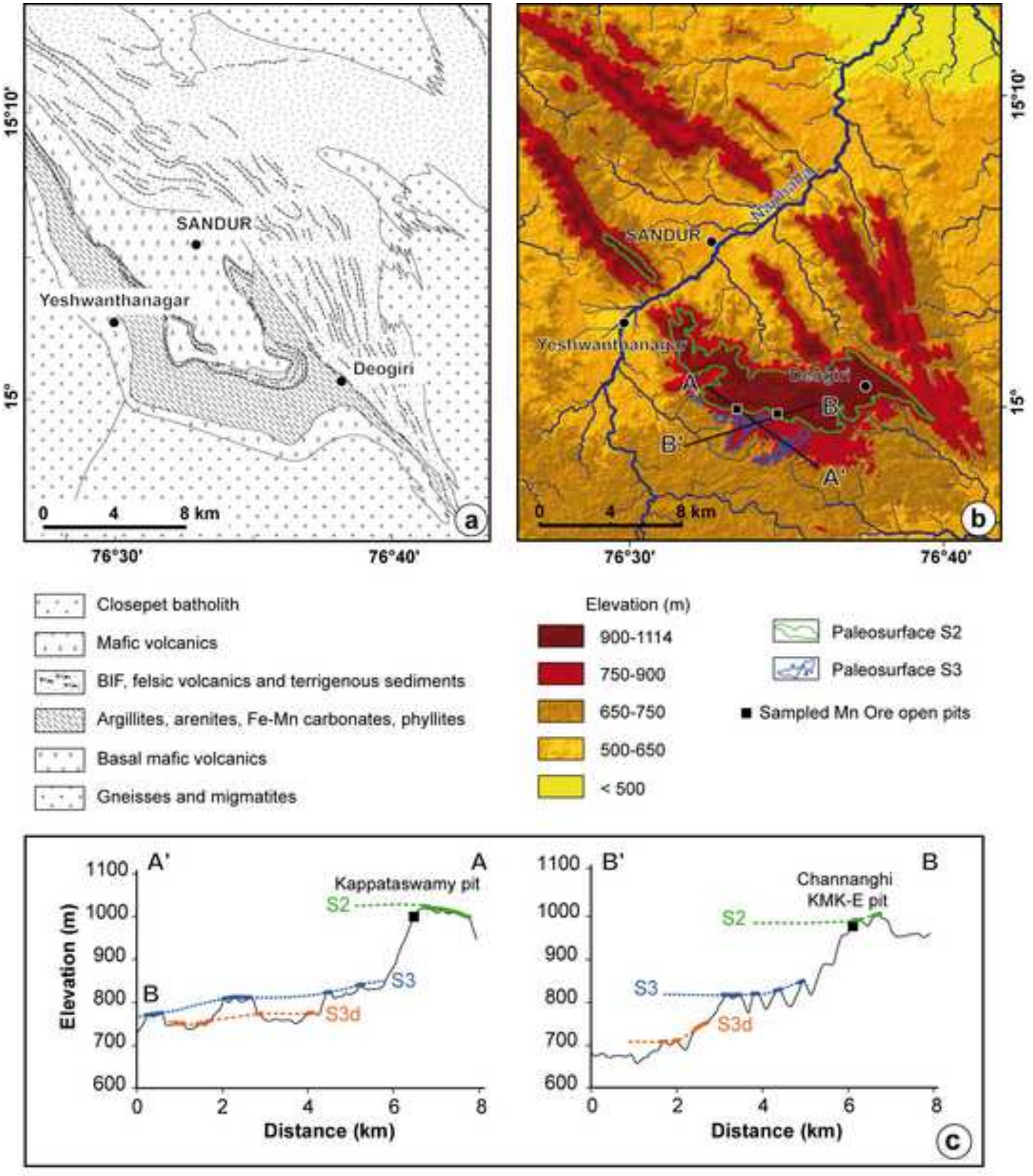

FIG. 2

Figure. 3
Click here to download high resolution image

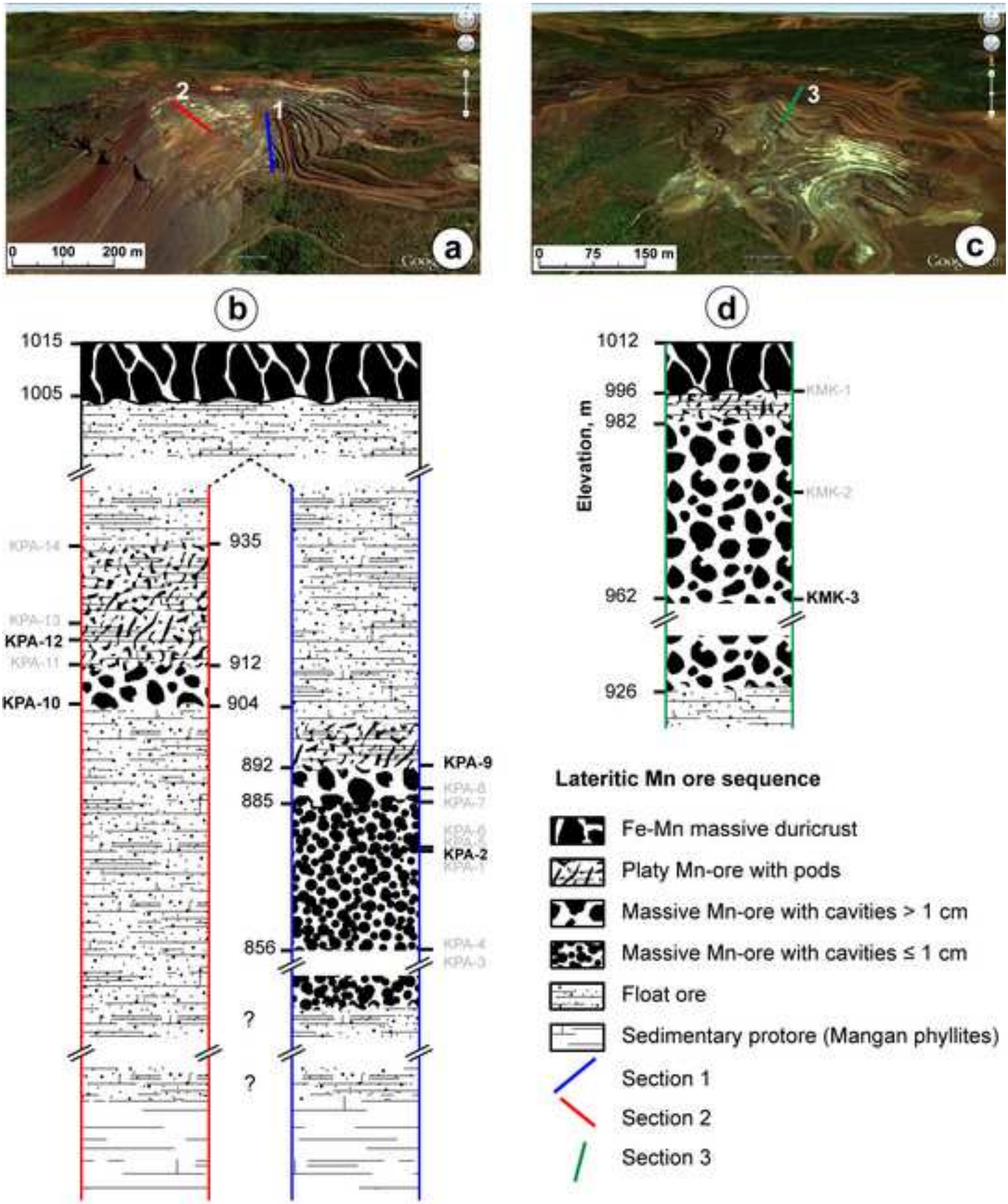

FIG. 3

Figure. 4

Click here to download high resolution image

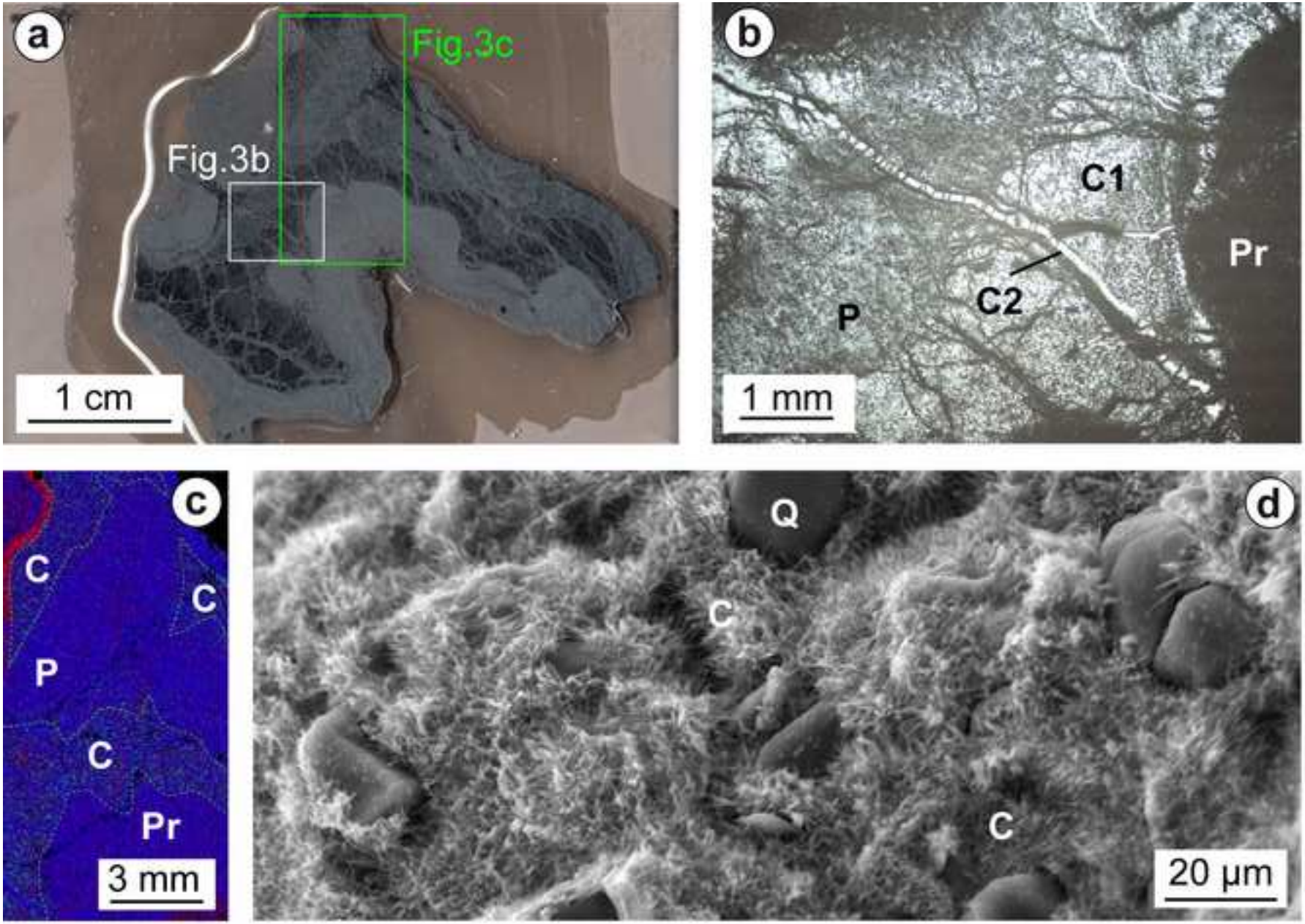

FIG. 4

Figure. 5

Click here to download high resolution image

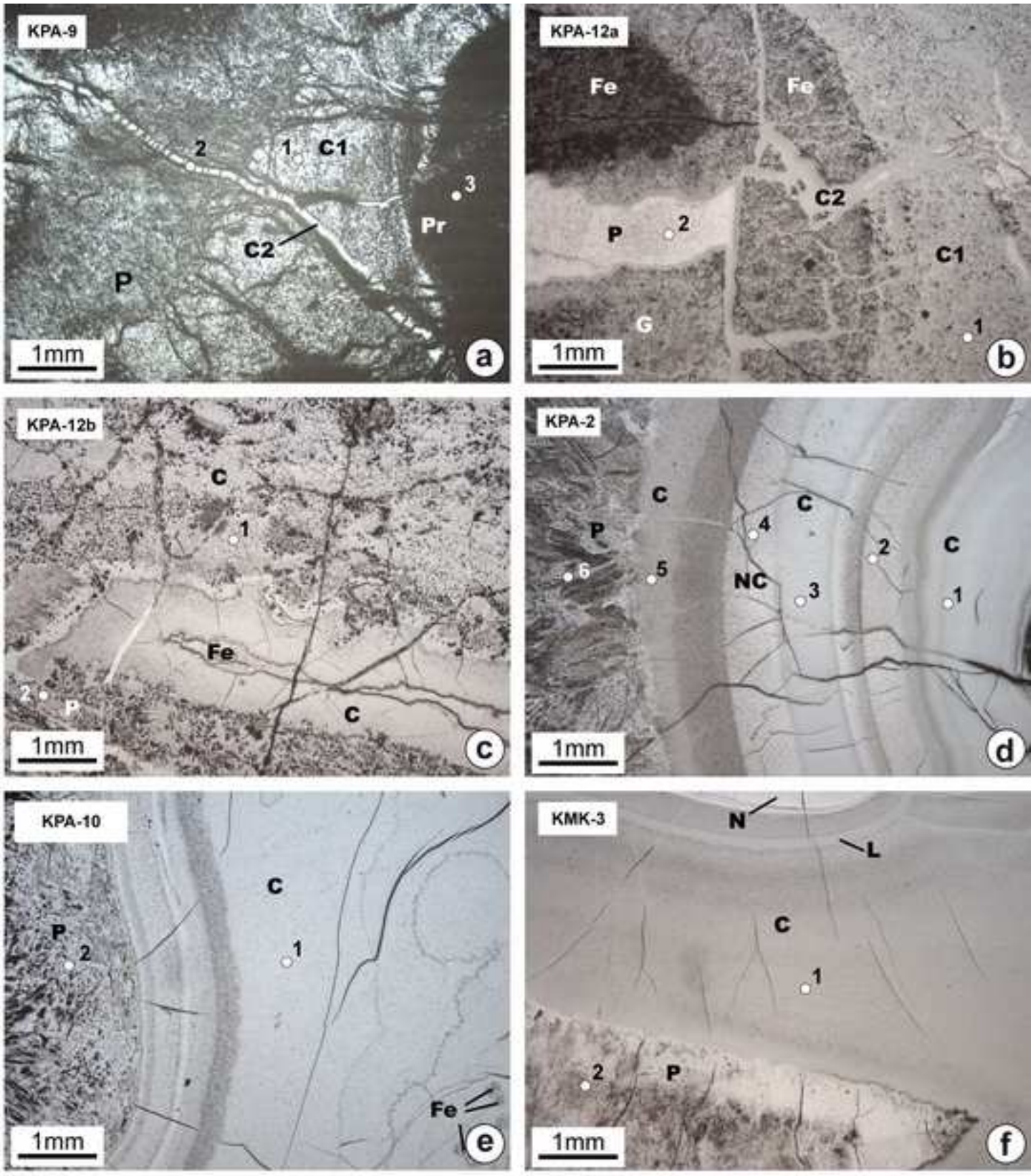

FIG. 5

Figure. 6

Click here to download Figure: FIgure. 6(EPSL-D-13-00742).pdf

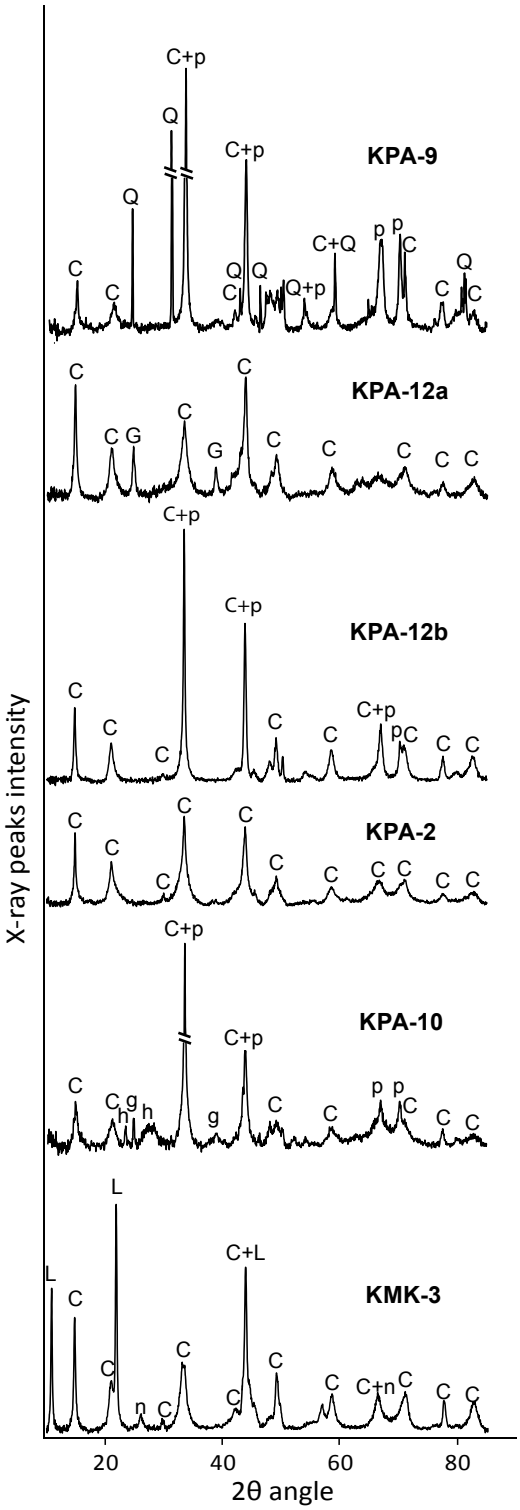

FIG. 6

Figure. 7

Click here to download Figure: Figure. 7(EPSL-D-13-00742).pdf

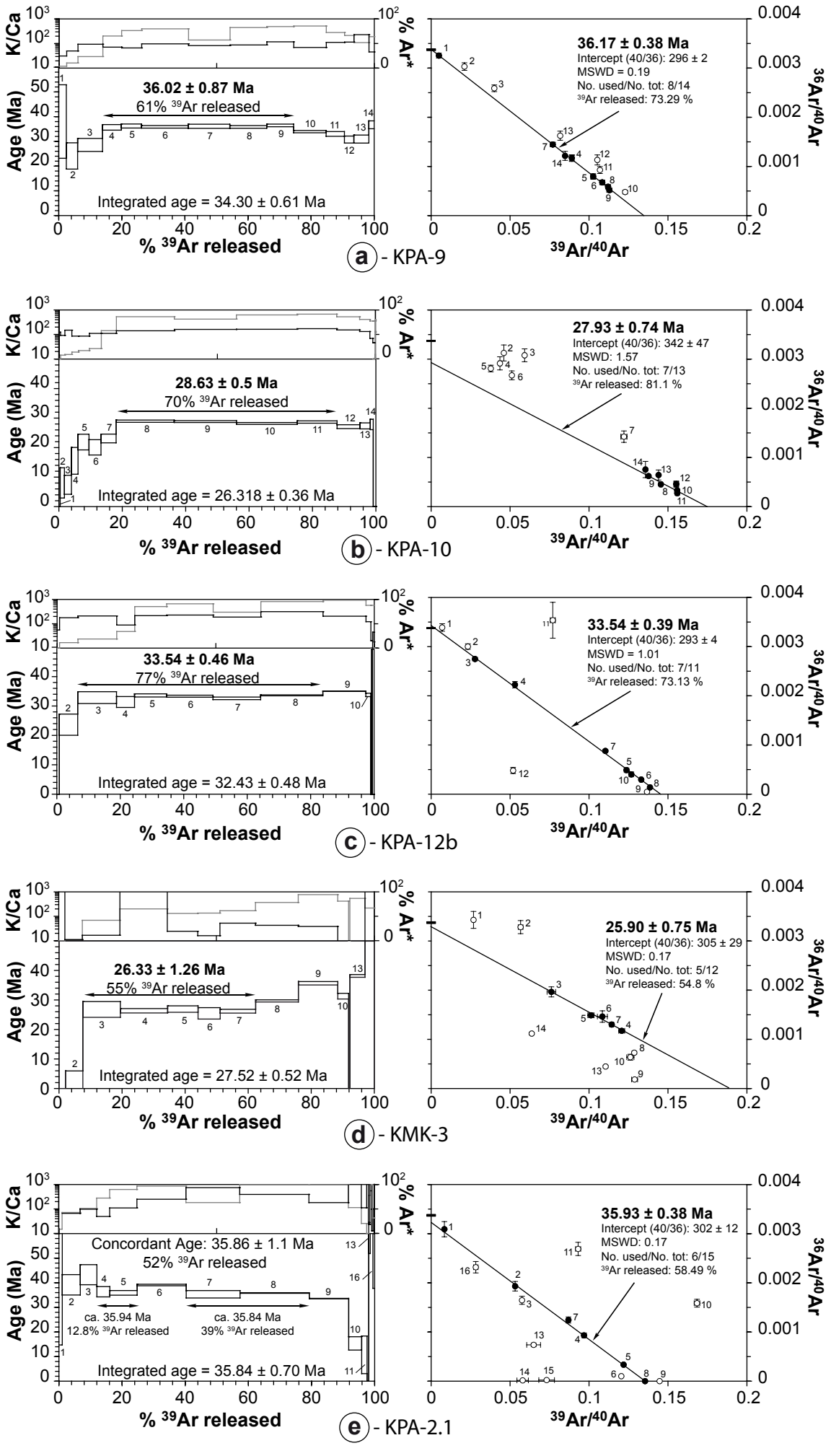

FIG. 7

Figure. 8

Click here to download Figure: Figure. 8(EPSL-D-13-00742).pdf

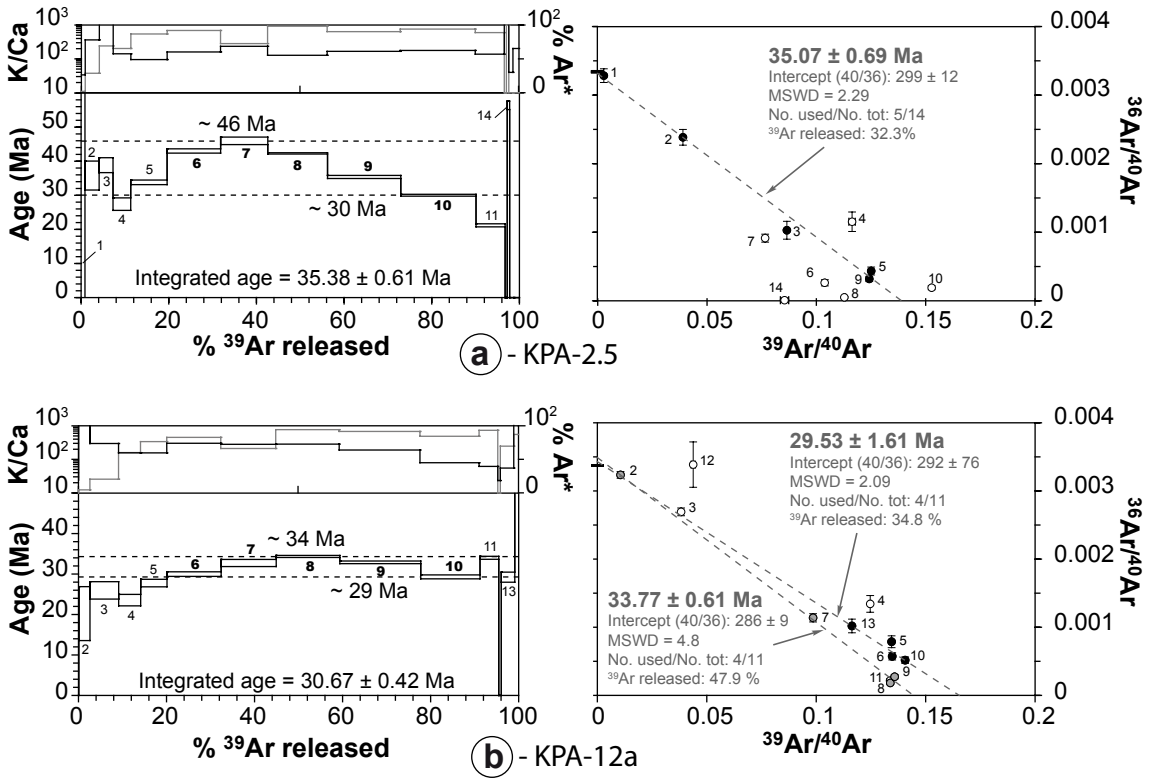

FIG. 8

Table. 1

Click here to download Table: Table. 1(EPSL-D-13-00742).doc

Sample ID	KMK-3		KPA-2						KPA-9			KPA-10		KPA-12a		KPA-12b	
	1	2	**1**	2	3	4	**5**	6	**1**	2	3	**1**	2	**1**	2	**1**	2
	C	P	**C**	C	C	C	**C**	P	**C**	C	Pr	**C**	P	**C**	P	**C**	P
wt. %																	
Mn	**60.15**	60.97	**59.72**	60.01	59.38	61.07	**59.13**	62.95	**56.62**	57.52	12.38	**59.11**	60.67	**59.10**	61.86	**59.82**	60.37
Al	**0.15**	0.30	**0.12**	0.30	0.22	0.33	**0.20**	0.00	**1.41**	1.24	0.37	**0.20**	0.29	**0.45**	0.11	**0.18**	0.37
Fe	**0.13**	0.13	**0.12**	0.13	0.13	0.13	**0.13**	0.14	**0.58**	0.51	0.17	**0.05**	0.13	**0.81**	0.14	**0.17**	0.85
K	**1.41**	0.06	**2.49**	2.26	2.44	0.94	**3.03**	-	**2.13**	2.19	0.50	**2.65**	0.87	**2.19**	0.19	**3.29**	0.29
Na	**0.03**	0.01	**0.09**	0.14	0.11	0.03	**0.08**	-	**0.06**	0.08	0.01	**0.10**	0.13	**0.08**	0.02	**0.07**	0.01
Zn	-	-	**0.01**	0.02	0.02	0.01	**0.02**	-	**0.01**	0.02	0.01	**0.01**	0.01	**0.01**	0.01	**0.01**	0.01
Co	-	-	-	-	-	0.01	-	-	**0.01**	0.01	0.01	-	0.01	**0.01**	-	**0.01**	0.01
Ba	**0.07**	0.02	**0.01**	-	-	0.01	**0.01**	0.01	**0.01**	0.01	-	**0.01**	-	-	0.01	**0.01**	0.02
Ni	-	-	-	-	-	-	-	-	-	-	-	-	-	-	-	-	-
Ti	-	-	-	-	-	-	-	-	**0.01**	0.01	-	-	-	-	-	-	-
Mg	-	0.00	**0.01**	0.01	0.01	0.01	**0.00**	-	**0.01**	0.01	-	**0.02**	0.01	**0.01**	-	**0.00**	0.02
Si	**0.06**	0.33	**0.07**	0.08	0.06	0.09	**0.07**	0.08	**0.38**	0.20	37.58	**0.06**	0.10	**0.08**	0.17	**0.07**	0.12
Ca	**0.02**	0.04	**0.12**	0.10	0.11	0.06	**0.11**	0.00	**0.11**	0.12	0.02	**0.18**	0.10	**0.11**	0.04	**0.13**	0.15
O	**35.59**	36.23	**35.60**	35.92	35.49	36.24	**35.44**	36.80	**35.35**	35.52	50.53	**35.36**	36.02	**35.68**	36.44	**35.89**	36.02
Total	**97.62**	98.11	98.36	98.98	97.99	98.92	**98.24**	99.99	**96.68**	97.41	101.6	**97.75**	98.35	**98.53**	98.99	**99.64**	98.24
Stoichiometric composition of cryptomelane based on 16 oxygens																	
K	**0.4**		**0.45**	0.41	0.45	0.17	**0.57**		**0.42**	0.4		**0.5**		**0.4**		**0.61**	
Mn^{IV}	**7.6**		**7.55**	7.59	7.55	7.83	**7.43**		**7.58**	7.6		**7.5**		**7.6**		**7.39**	
Mn^{III}	**0.4**		**0.45**	0.41	0.45	0.17	**0.57**		**0.42**	0.4		**0.5**		**0.4**		**0.61**	

- : not detected ; C = Cryptomelane ; P = Pyrolusite ; Pr = Si-Mn protore

Table. 1

Data repositories Tables

Click here to download Supplementary material for on-line publication only: DataRepositoryTables(EPSL-D-13-00742).pdf

Data repositories Main text

Click here to download Supplementary material for on-line publication only: Data repositories(EPSL-D-13-00742)-Main text.doc